

# Journal of Materials Chemistry A

Accepted Manuscript



This is an *Accepted Manuscript*, which has been through the Royal Society of Chemistry peer review process and has been accepted for publication.

*Accepted Manuscripts* are published online shortly after acceptance, before technical editing, formatting and proof reading. Using this free service, authors can make their results available to the community, in citable form, before we publish the edited article. We will replace this *Accepted Manuscript* with the edited and formatted *Advance Article* as soon as it is available.

You can find more information about *Accepted Manuscripts* in the [Information for Authors](#).

Please note that technical editing may introduce minor changes to the text and/or graphics, which may alter content. The journal's standard [Terms & Conditions](#) and the [Ethical guidelines](#) still apply. In no event shall the Royal Society of Chemistry be held responsible for any errors or omissions in this *Accepted Manuscript* or any consequences arising from the use of any information it contains.

Cite this: DOI: 10.1039/c0xx00000x

PAPER

www.rsc.org/xxxxxx

## Enhancement of Mineralization Ability of C<sub>3</sub>N<sub>4</sub> via lower Valence Position by Tetracyanoquinodimethane Organic Semiconductor

Mo Zhang, Wenqing Yao, Yanhui Lv, Xiaojuan Bai, Yanfang Liu, Wenjun Jiang and Yongfa Zhu\*

Received (in XXX, XXX) Xth XXXXXXXXXX 20XX, Accepted Xth XXXXXXXXXX 20XX

DOI: 10.1039/b000000x

7,7,8,8-Tetracyanoquinodimethane-g-C<sub>3</sub>N<sub>4</sub> (TCNQ-g-C<sub>3</sub>N<sub>4</sub>) organic composite photocatalysts were prepared by liquid ultrasonic route in water. The phenol mineralization ability of TCNQ-g-C<sub>3</sub>N<sub>4</sub> composite was dramatically enhanced via decreasing the valence position of the composite by adjusting the mass fraction of TCNQ. The transition of photogenerated electrons from the valence band of C<sub>3</sub>N<sub>4</sub> to the LUMO of TCNQ was promoted by the charge transfer between C<sub>3</sub>N<sub>4</sub> donor and TCNQ acceptor. The separation and immigration efficiency of photoinduced charge carriers was greatly enhanced and the catalytic activity of TCNQ-g-C<sub>3</sub>N<sub>4</sub> composite was increased about 8.4 times for phenol degradation.

### 1. Introduction

Graphitic carbon nitride (g-C<sub>3</sub>N<sub>4</sub>), with narrow band gap and chemical stability, has attracted much attention due to its potential application in energy and environment fields<sup>1-3</sup>. It is a promising visible light polymeric photocatalyst for remediation of environmental pollutants<sup>4</sup>, production of H<sub>2</sub> and O<sub>2</sub> from water<sup>5,6</sup> and photocatalytic conversion of CO<sub>2</sub><sup>7</sup>. Nevertheless, the application of g-C<sub>3</sub>N<sub>4</sub> in environmental protection is limited by its low mineralization ability for phenol pollutant due to its high valence position. Although the photocatalytic performance of g-C<sub>3</sub>N<sub>4</sub> can be improved via heteroatoms doping<sup>8-10</sup>, morphology controlling<sup>11-13</sup>, dyes sensitization<sup>14,15</sup> and hybrid fabrication<sup>16,17</sup>, there is hardly any efficiently enhanced mineralization ability of g-C<sub>3</sub>N<sub>4</sub> photocatalyst.

7,7,8,8-Tetracyanoquinodimethane (TCNQ) has a highly conjugated system and abundant  $\pi$  electrons, which is considered to be a powerful electron acceptor<sup>18,19</sup>. TCNQ and its anion have strong  $\pi$ - $\pi$  stacking interactions with carbon nanotubes and graphene<sup>20,21</sup>. Moreover, TCNQ is well-known to form charge-transfer (CT) complexes with extensive and novel electrical, electrochemical, and magnetic properties arising from the characteristic  $\pi$ -stacking of the TCNQ into the complexes<sup>22-25</sup>.

The conjugative  $\pi$  structure material hybridized photocatalysts exhibit enhanced photocatalytic activity due to rapid photoinduced charge separation<sup>26-31</sup>. In addition, the band structures of these semiconductor composites may be adjusted and the photocatalytic performance can be enhanced remarkably<sup>32</sup>.

Both of C<sub>3</sub>N<sub>4</sub> and TCNQ have conjugated structures and may achieve an ideal combination by their strong  $\pi$ - $\pi$  stacking interactions. Herein, the first example of TCNQ-C<sub>3</sub>N<sub>4</sub> photocatalyst is presented in this paper. Charge transfer is proved

to exist between TCNQ and C<sub>3</sub>N<sub>4</sub>. The valence position of the composite is successfully decreased by the CT interaction and the photocatalytic activity of TCNQ-C<sub>3</sub>N<sub>4</sub> is enhanced about 8.4 times for phenol degradation. This work provides a simple and low-cost method to synthesize the organic-semiconductor hybrids with controllable band structure, which show great potentials for application in photocatalysts, chemical sensors, and photovoltaic devices.

### 2. Experimental section

#### 2.1 Synthesis of photocatalyst

Dicyandiamide was purchased from Sinopharm Chemical Reagent Corp, P. R. China. All other reagents used in this research were analytically pure and used without further purification. The g-C<sub>3</sub>N<sub>4</sub> was prepared by pyrolysis of dicyandiamide in air atmosphere. The typical preparation of g-C<sub>3</sub>N<sub>4</sub> photocatalysts was as follows: 5 g of dicyandiamide was put in a Muffle Furnace and heated to 550 °C for 4 hours to complete the reaction. The yellow products were washed with nitric acid (0.1 mol·L<sup>-1</sup>) and deionized water to remove the residue absorbed on the surface of g-C<sub>3</sub>N<sub>4</sub>. Then the pure products were dried at 80 °C for 12 h.

The TCNQ-C<sub>3</sub>N<sub>4</sub> photocatalysts were prepared by liquid ultrasonic route in water. Firstly, the appropriate amount of C<sub>3</sub>N<sub>4</sub> was added into water and then was placed in an ultrasonic bath for 3 hours to completely disperse the C<sub>3</sub>N<sub>4</sub>. The TCNQ-DMF solution (5 mg·mL<sup>-1</sup>) was added into the above solution. The solution was placed in an ultrasonic bath for an hour and was stirred in a fume hood for 24 h. After volatilization of the solvent, the samples were dried at 80 °C. According to this method, different mass ratios of TCNQ-C<sub>3</sub>N<sub>4</sub> photocatalysts from 1% to 50% were synthesized.

## 2.2 Characterizations

The morphologies and structures of the samples were examined with HITACHI HT7700 transmission electron microscopy (TEM) operated at an accelerating voltage of 100 kV. UV-Vis diffuse reflectance spectroscopy (DRS) was carried out on a Hitachi U-3010 UV-vis spectrophotometer using BaSO<sub>4</sub> as the reference. The crystallinity of the as-prepared sample was characterized by X-ray diffraction (XRD) on Bruker D8-advance diffractometer using Cu-K $\alpha$  radiation ( $\lambda = 1.5418 \text{ \AA}$ ). The photocurrents were measured on an electrochemical system (CHI 660D, China). Raman spectra were obtained by using a HORIBA JY HR800 confocal microscope Raman spectrometer employing an Ar-ion laser (514.5 nm). A 50 $\times$  telephoto Olympus objective lens was used to focus the laser on the samples. All spectra were calibrated with respect to silicon wafer at 520.7 cm<sup>-1</sup>. Fourier transformed infrared (FTIR) spectra were recorded on a Bruker VERTEX 700 spectrometer. Photoluminescence spectra (PL) of the samples were obtained at room temperature using a HORIBA Aqualog Fluorescence Spectrometer.

## 2.3 Photocatalytic experiments

The photocatalytic activities were evaluated by the decomposition of phenol under visible light irradiation ( $\lambda > 420 \text{ nm}$ ) and simulated sunlight irradiation. Visible irradiation was obtained from a 500 W Xe lamp (Institute for Electric Light Sources, Beijing) with a 420 nm cutoff filter, and the average visible light intensity was 35 mW $\cdot$ cm<sup>-2</sup>. For the photocatalytic experiments, 25 mg of photocatalyst was totally dispersed in an aqueous solution of phenol (50 mL, 5 ppm). Before irradiation, the suspensions were magnetically stirred in the dark for 2 h to get absorption-desorption equilibrium between the photocatalyst and phenol. At certain time intervals, 3 mL aliquots were sampled and centrifuged to remove the particles. The concentration of phenol was analyzed by chromatographic experiments with HPLC-UV/vis system.

## 2.4 Analyses of the degradation intermediates for phenol

The chromatographic experiments with HPLC-UV/vis system were carried out using an ultraviolet absorbance detector (K 2501) operated at 275 nm for phenol, 285 nm for 2,4-dichlorophenol and 280 nm for bisphenol A coupled with a Venusil XBP-C18 (Agela Technologies Inc.) column. Before the analysis, the samples were filtered through millipore discs of 0.45  $\mu\text{m}$  to protect the chromatographic column. The mobile phase used for eluting pollutant and its degradation intermediates from the HPLC columns consisted of methanol and water (60:40 for phenol, 75:25 for 2,4-dichlorophenol and 70:30 for bisphenol A, v/v) at a flow rate of 1 mL $\cdot$ min<sup>-1</sup>.

## 2.5 Photoelectrochemical measurements

To investigate the transition of photogenerated electrons of TCNQ-g-C<sub>3</sub>N<sub>4</sub>, a standard three-electrode cell with a working electrode (as-prepared photocatalyst), a platinum wire as counter electrode, and a saturated calomel electrode (SCE) as reference electrode were used in the photoelectric studies. 0.1 M Na<sub>2</sub>SO<sub>4</sub> was used as the electrolyte solution. Potentials are given with reference to the SCE. The photoresponses of the photocatalysts as light on and off were measured at 0.0 V. The working electrodes

were prepared as follows: 5 mg of the as-prepared photocatalyst was suspended in 1 mL water to produce slurry, which was then dip-coated onto a 2 cm $\times$ 4 cm indium tin oxide (ITO) glass electrode. Electrodes were exposed to air atmosphere for 12 h to eliminate water and subsequently calcined at 100  $^{\circ}\text{C}$  for 5 hours.

## 3. Results and discussions

The TCNQ-C<sub>3</sub>N<sub>4</sub> photocatalysts were prepared by liquid ultrasonic route in water (Figure 1a). The pure g-C<sub>3</sub>N<sub>4</sub> exhibits bulk morphology and the TCNQ shows layered film morphology (Figure S1). With the increase of TCNQ mass fraction in the precursor, the g-C<sub>3</sub>N<sub>4</sub> is blended with TCNQ which is obscure at this resolution. Figure 1b, c shows HRTEM images of 10%-TCNQ-C<sub>3</sub>N<sub>4</sub> photocatalyst. The thickness of the TCNQ layer coated on the 10%-TCNQ-C<sub>3</sub>N<sub>4</sub> sample was about 10-20 nm. However, when the mass fraction of TCNQ is higher than 10%, the excessive TCNQ disperses in the water and fails to adhere to C<sub>3</sub>N<sub>4</sub> during the preparation process. The XRD patterns (Figure 2) indicate the crystal phase of C<sub>3</sub>N<sub>4</sub> did not change with increasing TCNQ content. There was no crystalline TCNQ in the TCNQ-C<sub>3</sub>N<sub>4</sub> photocatalysts with low TCNQ loadings. The as-prepared TCNQ-C<sub>3</sub>N<sub>4</sub> samples with higher TCNQ loadings (>5%) exhibited crystalline TCNQ peaks, and the peak intensities are enhanced with the increasing TCNQ loading. Thus, it can be inferred that TCNQ was dispersed uniformly on the C<sub>3</sub>N<sub>4</sub> surface with low TCNQ loadings, while crystalline TCNQ appeared only if its loading exceeded a threshold value (5%).

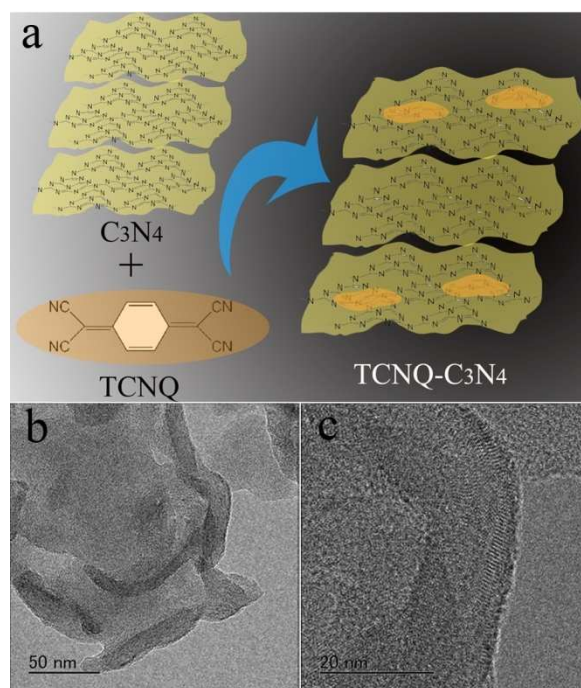


Figure 1 (a) Schematic illustration of preparation of TCNQ-C<sub>3</sub>N<sub>4</sub> composite. (b, c) The HRTEM images of 10%-TCNQ-C<sub>3</sub>N<sub>4</sub> catalyst.

Figure 3a and S2 shows the photocatalytic activity of C<sub>3</sub>N<sub>4</sub> and TCNQ-C<sub>3</sub>N<sub>4</sub> photocatalysts with different mass fraction of TCNQ under visible light and simulated sunlight irradiation. The photocatalytic rate constant is sharply enhanced with increasing

TCNQ content. When the mass fraction of TCNQ reaches 10%, the apparent rate constant  $k$  is almost 9.4 times as high as that of pure  $C_3N_4$ . However, as the proportion of TCNQ further increases, the degradation rate decreases gradually though it remains higher than that of  $C_3N_4$ . This change in photocatalytic activity of TCNQ- $C_3N_4$  may be attributed to the balance between

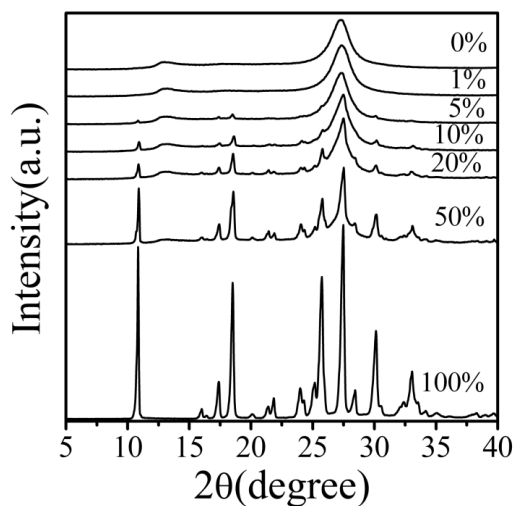


Figure 2 XRD spectra of g- $C_3N_4$ , pure TCNQ and TCNQ- $C_3N_4$  materials.

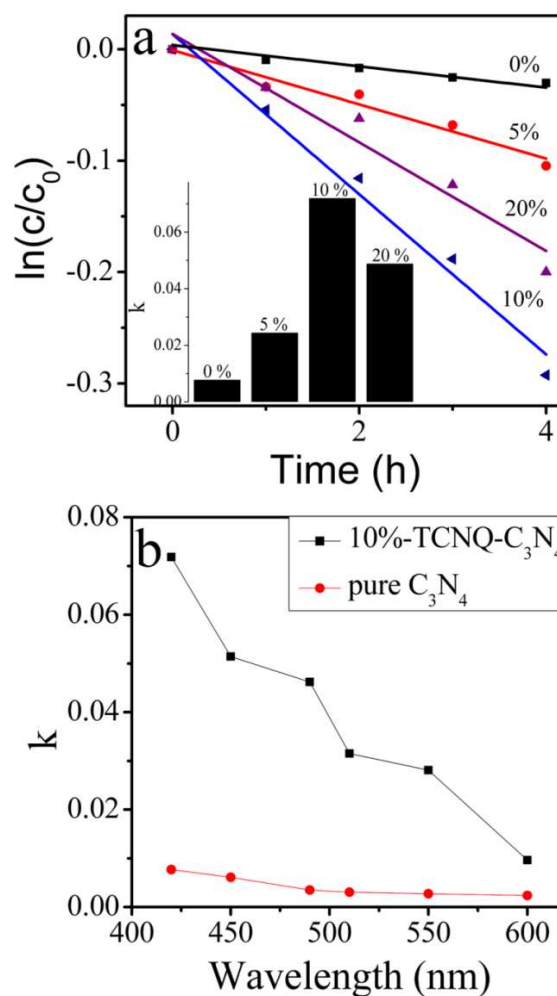


Figure 3 (a) Photocatalytic degradation of phenol, (inset) the apparent rate constants over pure g- $C_3N_4$  (0%) and TCNQ- $C_3N_4$  with different TCNQ mass fraction (5% ~ 20%) under visible light irradiation ( $\lambda > 420$  nm). (b) Wavelength dependence of degradation of phenol by 10%-TCNQ- $C_3N_4$  and pure  $C_3N_4$ .

charge separation and light harvesting. Although TCNQ is beneficial for charge separation of the TCNQ- $C_3N_4$  photocatalyst, it will shade  $C_3N_4$  at too much addition. In Figure 3b, the overall enhanced photocatalytic activity for phenol degradation is observed on 10%-TCNQ- $C_3N_4$  across the whole of its absorption spectrum. This wavelength-independent enhancement indicates there may be some interaction between TCNQ and  $C_3N_4$  that plays an important role in improving the photocatalytic activity. In addition, the photocatalytic activities of TCNQ- $C_3N_4$  for 2,4-dichlorophenol and bisphenol A degradation are also obviously enhanced. As shown in Figure S3, the photocatalytic rate constants of TCNQ- $C_3N_4$  are 3.4 and 2.3 times as high as pure  $C_3N_4$  for 2,4-dichlorophenol and bisphenol A degradation respectively.

The phenol photodegradation intermediates are investigated by chromatograms of phenol before and after photocatalytic degradation for 4h monitored at 275 nm (Fig S4). The peak at 5.3 min can be identified as phenol, the intensity of which was decreased during the constant photocatalytic reaction. The new peaks at lower retention times imply that phenol was oxidized to

several intermediates, including dihydroxybenzene, 4,4-dihydroxybiphenyl and maleic anhydride<sup>33,34</sup>. The higher intensity of intermediates by TCNQ-C<sub>3</sub>N<sub>4</sub> than pure C<sub>3</sub>N<sub>4</sub> indicate that the degradation ability of TCNQ-C<sub>3</sub>N<sub>4</sub> is remarkable enhanced and the intermediates could be further degraded by ring cleavage and finally subjected to completely degradation to CO<sub>2</sub> and H<sub>2</sub>O.

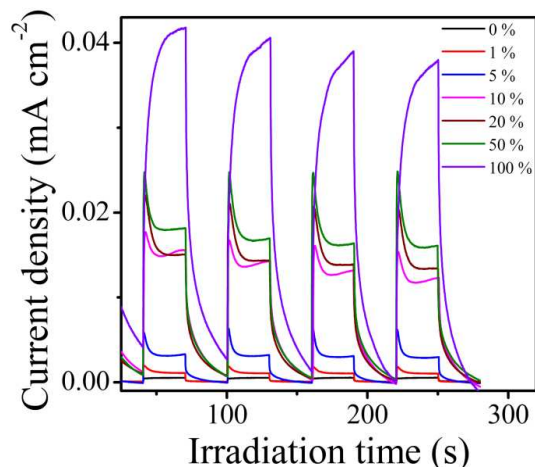


Figure 4 Photocurrents of pure g-C<sub>3</sub>N<sub>4</sub> (0%) and TCNQ-C<sub>3</sub>N<sub>4</sub> with different TCNQ mass fraction under visible light irradiation ( $\lambda > 420$  nm, [Na<sub>2</sub>SO<sub>4</sub>] = 0.1 M).

Photocurrents were measured for TCNQ-C<sub>3</sub>N<sub>4</sub> and C<sub>3</sub>N<sub>4</sub> electrodes to investigate the electronic interaction between TCNQ and C<sub>3</sub>N<sub>4</sub> (Figure 4). Under visible light irradiation, the photocurrent was remarkably enhanced along with the increase of TCNQ content. The photocurrent of 10%-TCNQ-C<sub>3</sub>N<sub>4</sub> was about 23 times as high as that of the pure C<sub>3</sub>N<sub>4</sub> electrode, which indicates that the separation and transition efficiency of photoinduced electrons and holes was improved via the interaction between TCNQ and C<sub>3</sub>N<sub>4</sub>. The photocurrent was enhanced continuously when the mass fraction of TCNQ further increases, which was different from the change of the photocatalytic activity. As the photocurrent is a long-term process and is limited by the carrier mobility<sup>35</sup>, the continuous enhancement in photocurrent can be attributed to the relatively higher carrier mobility of TCNQ than C<sub>3</sub>N<sub>4</sub>.

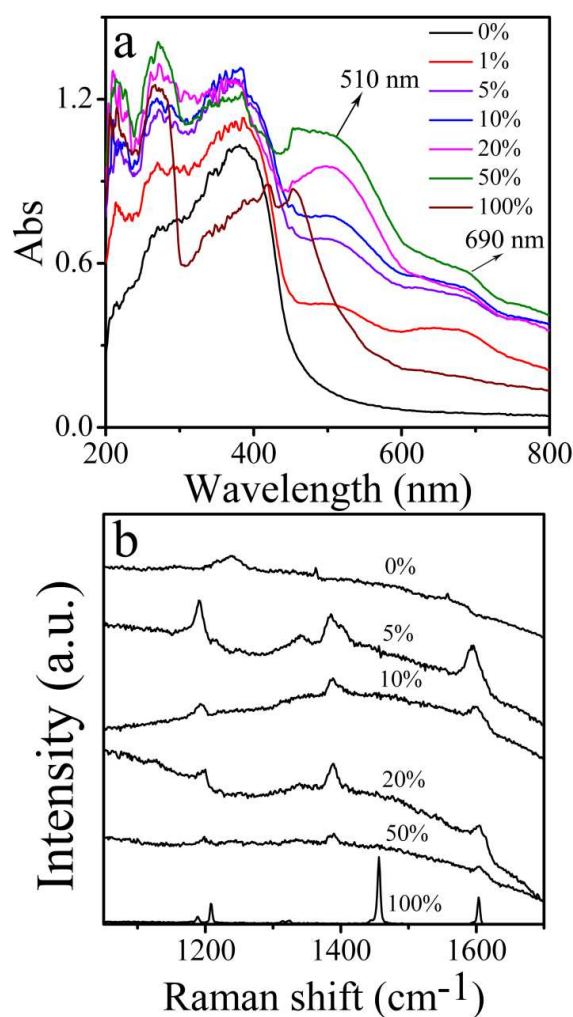


Figure 5 (a) UV-vis diffuse reflectance spectra of g-C<sub>3</sub>N<sub>4</sub> (0%), pure TCNQ (100%) and TCNQ-C<sub>3</sub>N<sub>4</sub> with different mass fraction of TCNQ (1% ~ 50%). (b) Raman spectra of g-C<sub>3</sub>N<sub>4</sub>, pure TCNQ and TCNQ-C<sub>3</sub>N<sub>4</sub> materials.

The UV-Vis DRS spectra (Figure 5a) show two charge-transfer bands of the C<sub>3</sub>N<sub>4</sub>-TCNQ at 510 nm and 690 nm. With increasing TCNQ content, remarkable enhanced charge-transfer absorption was observed, indicating the extended absorption of TCNQ-C<sub>3</sub>N<sub>4</sub> in visible light region and optimized band structure for charge migration and separation<sup>36</sup>. The typical Raman spectrum at 1355 and 1558 cm<sup>-1</sup> for g-C<sub>3</sub>N<sub>4</sub> are referred to presence of disorder in graphite (D band) and the in-plane bond-stretching motion of pairs of C sp<sup>2</sup> atoms (G band)<sup>37,38</sup> (Figure 5b). The principal vibration modes for TCNQ at 1208 cm<sup>-1</sup> (C=CH bending), 1603 cm<sup>-1</sup> (C=C ring stretching) downshift by about 16 and 4 cm<sup>-1</sup> respectively for 10%-TCNQ-C<sub>3</sub>N<sub>4</sub>. This low-frequency shift might be the result of increase in the conjugation length. In addition, the v<sub>4</sub> Raman bands (C=C wing stretching) of TCNQ<sup>0</sup> and TCNQ<sup>-1</sup> molecules are observed at around 1456 and 1388 cm<sup>-1</sup>, the frequency of which in TCNQ molecules varies with the degree of the charge transfer in TCNQ salt<sup>39</sup>. In addition, as presented in the IR spectra (Figure S5), the vibrational band at 1628 and 1231 cm<sup>-1</sup> for pure C<sub>3</sub>N<sub>4</sub> shift to 1632 and 1238 cm<sup>-1</sup> for the TCNQ-C<sub>3</sub>N<sub>4</sub> composites with increasing TCNQ content. The

blue shift in the stretching band evidences that  $C_3N_4$  is positively charged in the composite<sup>36, 40, 41</sup>. The obvious changes of the chemical structures for TCNQ- $C_3N_4$  photocatalysts indicate that charge transfer exists between them and photogenerated electrons may transit from  $C_3N_4$  to TCNQ.

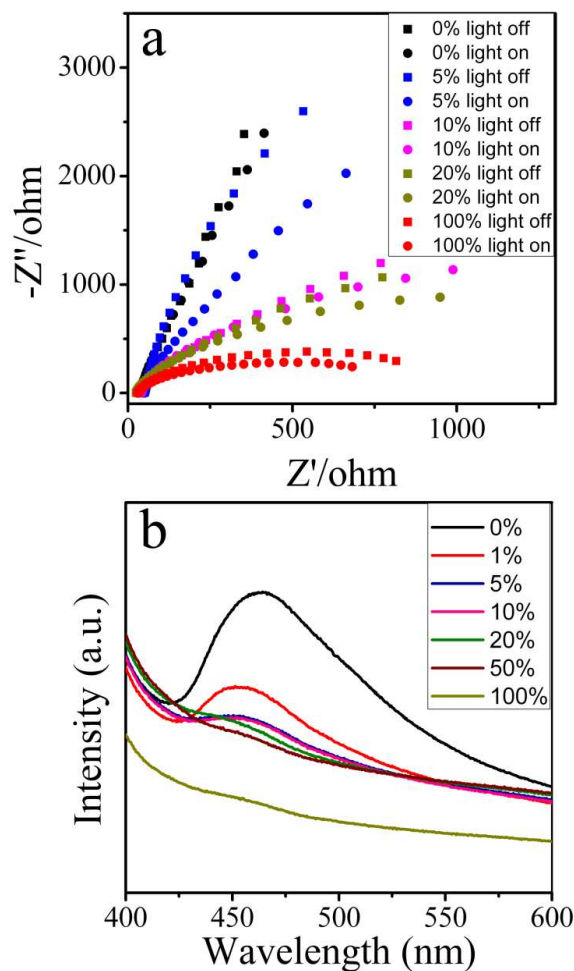


Figure 6 (a) EIS Nyquist plots of pure  $g\text{-}C_3N_4$  (0%), pure TCNQ (100%) and TCNQ- $C_3N_4$  with different TCNQ mass fraction (5% ~ 20 %). (b) Photoluminescence (PL) spectra of pure  $g\text{-}C_3N_4$  (0%), pure TCNQ (100%) and TCNQ- $C_3N_4$  with different TCNQ mass fraction (1% ~ 50 %).

The smaller arc radius on the electrochemical impedance spectroscopy (EIS) Nyquist plot of TCNQ- $C_3N_4$  with increased TCNQ content under visible light irradiation (Figure 6a) could be observed, indicating a more effective separation efficiency of photogenerated electron-hole pairs and a faster interfacial charge transfer. The arc radius on the EIS Nyquist plot of TCNQ- $C_3N_4$  was also smaller than that of  $C_3N_4$  without irradiation, suggesting that TCNQ changed the charge distribution of  $C_3N_4$  and made charge transfer easier. In addition, the arc radius on the EIS Nyquist plot of pure TCNQ is smaller than TCNQ- $C_3N_4$  photocatalysts and pure  $C_3N_4$ , which can attribute to the higher carrier mobility of TCNQ. This result implied that TCNQ could obviously favor the separation and transition of photogenerated carriers in TCNQ- $C_3N_4$  photocatalysts and enhanced the photocatalytic activity. In addition, the photoluminescence (PL)

intensity of TCNQ- $C_3N_4$  (Figure 6b) is decreased gradually with increasing TCNQ content, indicating that the relaxation of a fraction of TCNQ- $C_3N_4$  excitons may occur via charge transfer of electrons and holes rather than radiative paths<sup>42, 43</sup>. Thus, the lower recombination probability of photogenerated charge carriers for TCNQ- $C_3N_4$  compared to pure  $C_3N_4$  can be inferred.

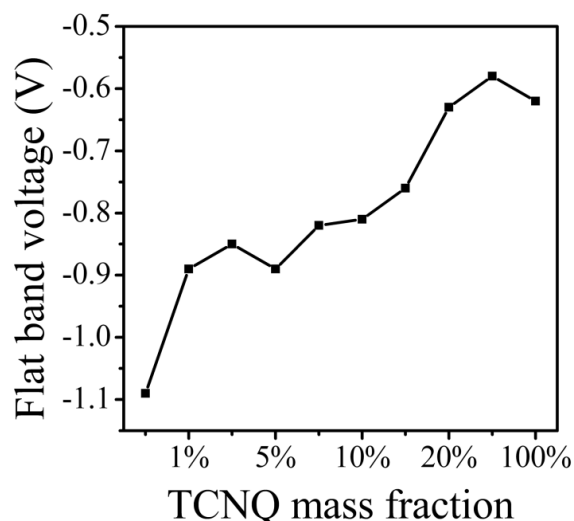


Figure 7 The derived flat-band potential for pure  $g\text{-}C_3N_4$  (0%), pure TCNQ (100%) and TCNQ- $C_3N_4$  with different TCNQ mass fraction (1% ~ 50 %)

The calculated flat band potential ( $V_{fb}$ ) for  $C_3N_4$  and TCNQ electrodes are -1.09 and -0.62 V versus SCE (Figure S6, 7), respectively<sup>5, 44</sup>. As shown in Figure 7, the  $V_{fb}$  of the TCNQ- $C_3N_4$  shifts to positive gradually with the increasing TCNQ content. A considerable change of band position of TCNQ- $C_3N_4$  can be deduced. TCNQ is a popular organic acceptor, so charge transfer may take place between  $C_3N_4$  and TCNQ when they are mixed through stacking. According to the simplest model of intermolecular charge transfer complex by Mulliken<sup>45</sup>, a fraction of electrons may transfer from the highest occupied molecular orbital (HOMO) of the donor to the lowest unoccupied molecular orbital (LUMO) of the acceptor in the electronic ground state. The decreased  $V_{fb}$  of the TCNQ- $C_3N_4$  indicate that more photogenerated holes may turn up when charges transfer from the HOMO of  $C_3N_4$  to the LUMO of TCNQ. The electronic structures of  $C_3N_4$ , TCNQ and TCNQ- $C_3N_4$  are further investigated by valence band spectra of X-ray photoelectron spectroscopy. As shown in Figure S8, the valence-band electronic structures of the pure  $C_3N_4$  and TCNQ are in reasonable agreement with the calculations. Thus, the band structures of the composites are changed and the oxidation capacity of the photogenerated holes may be enhanced (Figure 8).

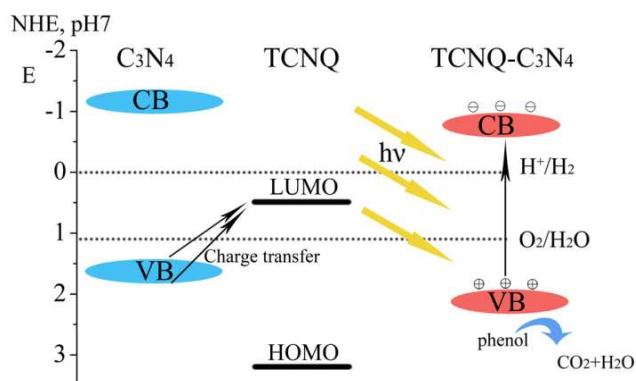


Figure 8 Schematic of band structure and photogenerated charge transfer of the TCNQ-g-C<sub>3</sub>N<sub>4</sub> material under visible light irradiation.

To confirm the mechanism further, electron spin resonance (ESR) technique and radical trapping experiment were performed. As shown in Figure S9, a gradual evolution of ESR signals for DMPO-O<sub>2</sub><sup>•-</sup> adducts in H<sub>2</sub>O for 10%-TCNQ-C<sub>3</sub>N<sub>4</sub> was observed with visible light irradiation, indicating the generation of a spot of superoxide radical under visible light. None of DMPO-•OH adducts was detected. However, the obvious DMPO-O<sub>2</sub><sup>•-</sup> and DMPO-•OH signal under visible light was observed for pure C<sub>3</sub>N<sub>4</sub>, which means the presence of superoxide radical and hydroxyl radical during the photocatalytic process. The different ESR signals for pure C<sub>3</sub>N<sub>4</sub> and 10%-TCNQ-C<sub>3</sub>N<sub>4</sub> indicate their different photodegradation mechanism. Figure S10 shows the photodegradation of phenol with the addition of hydroxyl radical scavenger (tBuOH), hole scavenger (EDTA-2Na) and N<sub>2</sub> under visible light irradiation<sup>46, 47</sup>, respectively. The photocatalytic activity of 10%-TCNQ-C<sub>3</sub>N<sub>4</sub> decreases slightly by the addition of hydroxyl radical scavenger but reduces greatly with the addition of hole radical scavengers, indicating that the holes are the main oxidative species for 10%-TCNQ-C<sub>3</sub>N<sub>4</sub> sample. Moreover, the photocatalytic activity of 10%-TCNQ-C<sub>3</sub>N<sub>4</sub> also decreases and the color of the reaction system solution turns blue when continuous nitrogen gas is bubbled in the solution to restrain the production of •O<sub>2</sub>. It can be inferred that •O<sub>2</sub> is also an oxidative species for 10%-TCNQ-C<sub>3</sub>N<sub>4</sub> and the transferred charges on the HOMO of TCNQ cannot react with O<sub>2</sub> to produce •O<sub>2</sub> in the reaction system with continuous nitrogen gas. Therefore, the TCNQ gains electrons and becomes the negative ion, which shows blue in the solution. Figure S10b shows the photocatalytic activity of pure C<sub>3</sub>N<sub>4</sub> decreases slightly by the addition of hole radical scavengers but reduces greatly with the addition of hydroxyl radical scavenger and N<sub>2</sub>, indicating that the hydroxyl radical and •O<sub>2</sub> are the main oxidative species for C<sub>3</sub>N<sub>4</sub>. As shown in Figure S10, the different photodegradation mechanism of pure C<sub>3</sub>N<sub>4</sub> and 10%-TCNQ-C<sub>3</sub>N<sub>4</sub> indicate that the band structure of TCNQ-C<sub>3</sub>N<sub>4</sub> is changed by the introduction of TCNQ and the oxidation capacity of the photogenerated holes is greatly enhanced by that.

#### 4. Conclusions

In summary, the TCNQ-C<sub>3</sub>N<sub>4</sub> photocatalysts have been prepared by liquid ultrasonic route in water. Compared with pure g-C<sub>3</sub>N<sub>4</sub>,

the valence band position of TCNQ-C<sub>3</sub>N<sub>4</sub> was obviously decreased and the phenol mineralization ability of TCNQ-C<sub>3</sub>N<sub>4</sub> was remarkably enhanced. This work develops new space for the preparation of promising composites with controllable band structures and their application in degradation of organic pollutants.

#### Acknowledgements

This work was partly supported by National Basic Research Program of China (973 Program) (2013CB632403), National High Technology Research and Development Program of China (2012AA062701) and Chinese National Science Foundation (20925725 and 21373121).

#### Notes and references

Department of Chemistry, Beijing Key Laboratory for Analytical Methods and Instrumentation, Tsinghua University, Beijing, 100084, China. Fax: (+86)10-6278-7601; Tel: (+86)10-6278-3586;

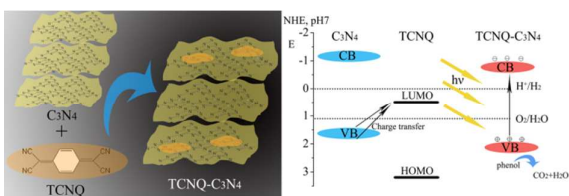
E-mail: zhuoyf@mail.tsinghua.edu.cn

† Electronic Supplementary Information (ESI) available: [details of any supplementary information available should be included here]. See DOI: 10.1039/b000000x/

- X. Chen, S. Shen, L. Guo, S. S. Mao, *Chem. Rev.* 2010, **110**, 6503.
- Y. Wang, X. Wang, M. Antonietti, *Angew. Chem. Int. Ed.* 2012, **51**, 68.
- Y. Zheng, J. Liu, J. Liang, M. Jaroniec, S. Z. Qiao, *Energy Environ. Sci.* 2012, **5**, 6717.
- J. Xu, L. Wang, Y. Zhu, *Langmuir* 2012, **28**, 8418.
- X. Wang, K. Maeda, A. Thomas, K. Takanabe, G. Xin, J. M. Carlsson, K. Domen, M. Antonietti, *Nat. Mater.* 2009, **8**, 76.
- X. Wang, K. Maeda, X. Chen, K. Takanabe, K. Domen, Y. Hou, X. Fu, M. Antonietti, *J. Am. Chem. Soc.* 2009, **131**, 1680.
- Z. Huang., Li, F.; Chen, B.; Lu, T.; Yuan, Y.; Yuan, G. *Appl. Catal. B* 2013, **136–137**, 269.
- G. Liu, P. Niu, C. Sun, S. C. Smith, Z. Chen, G. Q. Lu, H. M. Cheng, *J. Am. Chem. Soc.* 2010, **132**, 11642.
- X. Chen, J. Zhang, X. Fu, M. Antonietti, X. Wang, *J. Am. Chem. Soc.* 2009, **131**, 11658.
- X. Wang, X. Chen, A. Thomas, X. Fu, M. Antonietti, *Adv. Mater.* 2009, **21**, 1609.
- X. H. Li, J. Zhang, X. Chen, A. Fischer, A. Thomas, M. Antonietti, X. Wang, *Chem. Mater.* 2011, **23**, 4344.
- S. S. Park, S. W. Chu, C. Xue, D. Zhao, C. S. Ha, *J. Mater. Chem.* 2011, **21**, 10801.
- J. Xu, Y. Wang, Y. Zhu, *Langmuir* 2013, **29**, 10566.
- K. Takanabe, K. Kamata, X. Wang, M. Antonietti, J. Kubota, K. Domen, *Phys. Chem. Chem. Phys.* 2010, **12**, 13020.
- S. Min, G. Lu, *J. Phys. Chem. C* 2012, **116**, 19644.
- L. Ge, C. Han, *Appl. Catal. B* 2012, **117–118**, 268.
- X. Bai R., Zong, C. Li, D. Liu, Y. Liu, Y. Zhu, *Appl. Catal. B* 2014, **147**, 82.
- D. S. Acker, R. J. Harder, W. R. Hertler, W. Mahler, L. R. Melby, R. E. Benson, W. E. Mochel, *J. Am. Chem. Soc.* 1960, **82**, 6408.
- N. Martin, J. L. Segura, C. J. Seoane, *Mater. Chem.* 1997, **7**, 1661.
- C. L. Hsu, C. T. Lin, J. H. Huang, C. W. Chu, K. H. Wei, L. J. Li, *ACS Nano* 2012, **6**, 5031.
- R. Hao, W. Qian, L. Zhang, Y. Hou, *Chem. Commun.* 2008, **48**, 6576.
- G. J. de A. A. Soler-Illia, C. Sanchez, B. Lebeau, Patarin, J. *Chem. Rev.* 2002, **102**, 4093.
- X. Chi, C. Besnard, V. K. Thorsmølle, V. Y. Butko, A. J. Taylor, T. Siegrist, A. P. Ramirez, *Chem. Mater.* 2004, **16**, 5751.
- X. Guégano, A. L. Kanibolotsky, C. Blum, S. F. L. Mertens, S. X. Liu, A. Neels, H. Hagemann, P. J. Skabara, S. Leutwyler, T. Wandlowski, A. Hauser, S. Decurtins, *Chem. Eur. J.* 2009, **15**, 63.

- 25 J. Lu, X. Qu, G. Peleckis, J. F. Boas, A. M. Bond, L. L. Martin, *J. Org. Chem.* 2011, **76**, 10078.
- 26 S. Vadahanambi, S. H. Lee, W. J. Kim, I. K. Oh, *Environ. Sci. Technol.* 2013, **47**, 10510.
- 5 27 L. Ge, C. Han, J. Liu, *J. Mater. Chem.* 2012, **22**, 11843.
- 28 X. H. Li, J. S. Chen, X. Wang, J. Sun, *J. Am. Chem. Soc.* 2011, **133**, 8074.
- 29 Q. Xiang, J. Yu, M. Jaroniec, *J. Phys. Chem. C* 2011, **115**, 7355.
- 30 L. W. Zhang, H. B. Fu, Y. F. Zhu, *Adv. Funct. Mater.* 2008, **18**, 2180.
- 10 31 Bai, X.; Wang, L.; Zong, R.; Lv, Y.; Sun, Y.; Zhu, Y. *Langmuir* 2013, **29**, 3097.
- 32 J. Zhang, M. Zhang, R. Q. Sun, X. Wang, *Angew. Chem.* 2012, **124**, 10292.
- 33 L. Liu, H. Liu, Y. P. Zhao, Y. Wang, Y. Duan, G. Gao, M. Ge, W. Chen, *Environ. Sci. Technol.* 2008, **42**, 2342.
- 15 34 Y. Liu, Y. Zhu, J. Xu, X. Bai, R. Zong, Y. Zhu, *Appl. Catal. B* 2013, **142–143**, 561.
- 35 Y. Liu, C. Xie J., Li, T. Zou, D. Zeng, *Appl. Catal. A* 2012, **433–434**, 81.
- 20 36 X. Mei, J. Ouyang, *Langmuir* 2011, **27**, 10953.
- 37 A. C. Ferrari, J. Robertson, *Phys. Rev. B* 2000, **61**, 14095.
- 38 P. V. Zinin, L. C. Ming, S. K. Sharma, V. N. Khabashesku, X. Liu, S. Hong, S. Endo, T. Acosta, *Chem. Phys. Lett.* 2009, **472**, 69.
- 39 M. Yoshikawa, S. Nakashima, A. Mitsuishi, *J. Raman Spectrosc.* 1986, **17**, 369.
- 25 40 R. Rathore, S. V. Lindeman, J. K. Kochi, *J. Am. Chem. Soc.* 1997, **119**, 9393.
- 41 K. Yakushi, K. Yamamoto, M. Simonyan, J. Ouyang, C. Nakano, Y. Misaki, K. Tanaka, *Phys. Rev. B* 2002, **66**, 235102.
- 30 42 M. Shalom, S. Inal, C. Fettkenhauer, D. Neher, M. Antonietti, *J. Am. Chem. Soc.* 2013, **135**, 7118.
- 43 L. Ge, C. Han, J. Liu, Y. Li, *Appl. Catal. A* 2011, **409–410**, 215.
- 44 S. Wen, W. Q. Deng, K. L. Han, *Chem. Commun.* 2010, **46**, 5133.
- 45 R. S. Mulliken, *J. Am. Chem. Soc.* 1952, **74**, 811.
- 35 46 H. Lee, W. Choi, *Environ. Sci. Technol.* 2002, **36**, 3872.
- 47 J. Zhou, C. Deng, S. Si, Y. Shi, X. Zhao, *Electrochim. Acta* 2011, **56**, 2062.





The phenol mineralization ability of TCNQ-g-C<sub>3</sub>N<sub>4</sub> is enhanced by the lower valence position and the charge transfer.